

Comparison between time-domain and frequency-domain Bayesian inferences to inspiral-merger-ringdown gravitational-wave signals

Hai-Tian Wang^{1,*} and Lijing Shao^{1,2,†}

¹*Kavli Institute for Astronomy and Astrophysics, Peking University, Beijing 100871, China*

²*National Astronomical Observatories, Chinese Academy of Sciences, Beijing 100012, China*

(Dated: January 26, 2024)

Time-domain (TD) Bayesian inference is important in ringdown analysis for gravitational wave (GW) astronomy. The validity of this method has been well studied by Isi and Farr [1]. Using GW190521 as an example, we study the TD method in detail by comparing it with the frequency-domain (FD) method as a complement to previous study. We argue that the autocovariance function (ACF) should be calculated from the inverse fast Fourier transform of the power spectral density (PSD), which is usually estimated by the Welch method. In addition, the total duration of the GW data that are used to estimate the PSD and the slice duration of the truncated ACF should be long enough. Only when these conditions are fully satisfied can the TD method be considered sufficiently equivalent to the FD method.

I. INTRODUCTION

Gravitational wave (GW) events detected by the LIGO-Virgo-KAGRA (LVK) Collaboration [2–4] give us an extraordinary opportunity to probe the gravitational physics in the strong field. The information of these GW events is hidden in the sea of noise introduced by the detector itself, the surrounding environment, artificial activities, and so on [5]. To extract information from GW data, we usually perform Bayesian inference in the frequency domain (FD). Note that the raw data detected by the detectors are in the time domain (TD). Therefore, we need to perform a fast Fourier transform (FFT) on the raw data for analysis in the FD. The FFT requires GW data to be infinitely long or periodic on the boundary, otherwise it may be affected by artifacts such as spectral leakage. For signals that do not satisfy these conditions, such as the ringdown signal which has a sharp start, TD Bayesian inference has been developed [6].

The ringdown signal is the final stage of a GW signal and is emitted by the oscillation of the remnant. It is described by the quasinormal modes (QNMs) and decays very quickly. It is usually expressed in the form of superimposed damped sinusoids [7–9]. Therefore, the ringdown signal is short enough to adopt the TD method, which is, for long signals, usually limited by the computational cost of solving the matrix inversion. In parallel, there are some investigations which developed different approaches to perform the FD Bayesian inference on the ringdown signal [10–13].

Interestingly, Isi *et al.* [14] and Cotesta *et al.* [15] come to different conclusions, while there are only some technical differences in the handling of the TD method. The former team analyzed the ringdown signal of GW150914 [16] with a sampling rate of 2048 Hz and a slice duration of 0.5 s, and they found evidence for the first overtone

mode with 3.6σ confidence. The latter team analyzed the same ringdown signal, but with a different sampling rate of 16 kHz and a different slice duration of 0.1 s, and they demonstrated that the “*claims of an overtone detection are noise dominated*”. In addition, there are some other technical details that can affect the results of the TD method, such as the total duration of the GW data used to estimate the power spectral density (PSD). It is challenging to conclude which setting is superior without knowing true values with TD methods alone. Comparisons made with FD results on ringdown signals remain inconclusive as it is affected by the previously mentioned sharp-edge effects in FFT.

However, such a comparison is possible for the full inspiral-merger-ringdown (IMR) signal of short duration, for example, in the GW190521 event [17]. The duration of GW190521 is about 0.1 s, which is sufficiently short for both FD and TD methods. We therefore compare results of the signal-to-noise ratio (SNR) and the Bayesian inference for these two methods, varying settings with different technical details. We find that the results of the TD method agree well with those of the FD method only if some specific setting is used.

Apart from the studies mentioned above, the TD method has been widely used to test the no-hair theorem [18], the black-hole area law [14], non-Kerr parameters [19–23], and black-hole thermodynamics [24]. Although Isi and Farr [6] have already studied this method in detail, our study here can be seen as a complement. It is important for the ongoing LVK observing runs and future GW detectors such as Einstein Telescope [25], Cosmic Explorer [26], Laser Interferometer Space Antenna [27], TianQin [28, 29], and Taiji [30].

This paper is organised as follows. In Sec. II and Sec. III, we show comparisons of noise and SNR estimations, respectively. In Sec. IV, we show results of Bayesian inference from the TD method and the FD method. In Sec. V, we provide a brief summary and some discussion. Throughout the paper, unless otherwise specified, we adopt geometric units where $G = c = 1$.

* Corresponding author: wanght@pku.edu.cn

† Corresponding author: lshao@pku.edu.cn

II. NOISE ESTIMATIONS

We use GW data provided by the Gravitational-Wave Open Science Center¹ [3]. There are several options for the raw data, and we obtained the data with a duration of 4096 s at a sampling rate of 16 kHz. We can later truncate it to the length that we need or resample it to a lower sampling rate. For the resampling algorithm, we use the one with the **Butterworth filter**, which is implemented in PyCBC (version 2.0.5) [31]. In this study, we estimate the autocovariance function (ACF) using different durations (d_T) and sampling frequencies (f_s).

We assume that the noise around GW190521 is Gaussian and stationary after applying a high-pass filter at $f_{\text{low}} = 20$ Hz. Specifically, we use the **Finite Impulse Response** filter [32] with an order of 512. We then estimate the one-sided PSD from downsampled data using the Welch method [33] and the *inverse spectrum truncation* algorithm. Note that all algorithms used above are implemented in the PyCBC package [31].

After the implementation of the high-pass filter, the noise can be well characterised by its PSD or ACF. There are three solutions to estimate the noise. Firstly, in the FD method, the one-side PSD ($S_n(f)$) is estimated with the Welch method [33] and the *inverse spectrum truncation* algorithm, which are implemented in the PyCBC package [31]. In this case, the inner product of two signals $h_1(f)$ and $h_2(f)$ is

$$\langle h_1(f) | h_2(f) \rangle = 4 \int_{f_{\text{low}}}^{f_s/2} \frac{h_1^*(f) h_2(f)}{S_n(f)} df, \quad (1)$$

where the asterisk in the upper right corner of $h_1(f)$ represents the complex conjugate of the signal. The inner product is important since it determines the way to calculate SNRs and likelihoods.

Then, there are two distinct TD methods, namely TTD1 and TTD2, employed in this study. Both methods utilize the same TD inner product, which is defined as

$$\langle h_1(t) | h_2(t) \rangle = h_1(t) \mathcal{C}^{-1} h_2^{\top}(t). \quad (2)$$

Herein, \top located at the upper right corner of $h_2(t)$ gives the transpose of the signal, which is a discrete vector in real GW data analysis. The difference between these two methods arises from their respective computation approaches for the covariance matrix \mathcal{C} . Note that the covariance matrix is determined by the ACF.

The ACF of the TTD1 method is estimated from GW data directly,

$$\begin{aligned} \mathcal{C}(k\Delta t) &= E[n(t) * n(t - k\Delta t)] \\ &= \frac{1}{K} \sum_{j=0}^{K-k} n(j\Delta t) n((j+k)\Delta t), \end{aligned} \quad (3)$$

where K is the total number of data samples, $0 \leq k \leq K - 1$, $E[\cdot]$ denotes the expectation value, $n(t)$ represents discrete noise samples, and Δt is the time intervals between samples. In this work, following Cotesta *et al.* [15], we calculate ACF using the `get_acf` function from `ringdown` (version 0.1) package [6].

The ACF of the TTD2 method is estimated according to the Wiener-Khinchin theorem. One can calculate it from the one-side PSD, $S_n(f)$, via

$$\begin{aligned} \mathcal{C}(\tau) &= 2 \int_{f_{\text{low}}}^{\infty} S_n(f) e^{2\pi i f \tau} df \\ &= 2 \sum_{f_{\text{low}}}^{f_s/2} S_n(f) e^{2\pi i f \tau} \Delta f, \end{aligned} \quad (4)$$

where $\tau = k\Delta t$. Note that the PSD is the same as that in the FD method.

As elucidated by Isi and Farr [6], the duration of ACFs derived from Eq. (3) and Eq. (4) ought to exceed the intended analysis duration. Consequently, it becomes necessary to truncate these ACFs to our required duration. For instance, while the inner product employs a duration $d_T = 0.5$ s, the estimated ACF's length from Eq. (4) is 4 s. We then proceed to truncate this 4-s long ACF and retain only its initial segment with a span of 0.5 s. This approach may yield results that deviate unexpectedly for both FD method and TTD2 method if not properly executed since the truncated ACF has less information than that of the original PSD.

For clarification, we summarize differences of these three methods as follows:

- **FD:** The PSD is estimated with the Welch method. In this work, we use the one implemented in the PyCBC package. The definition of the inner product is shown in Eq. (1).
- **TTD1:** The ACF is estimated according to Eq. (3). In this work, we estimate it with the `get_acf` function of the `ringdown` package. The definition of the inner product is shown in Eq. (2).
- **TTD2:** The ACF is estimated according to Eq. (4). In this work, we use the Welch method and the *inverse spectrum truncation* algorithm implemented in the PyCBC package. The definition of the inner product is shown in Eq. (2).

III. COMPARISONS

We have introduced the differences in noise estimation between the FD and TD methods. We then perform the Kolmogorov-Smirnov (KS) test on different methods to see which one gives a better estimate of the noise. We also show the results of SNRs based on these noise estimates.

¹ <https://gwosc.org/>

A. KS tests

To find an appropriate setting for the TD method, we perform the KS test for the TD and FD methods with different settings. The basic idea of the KS test is to evaluate the credible level at which the whitened noise is consistent with a normal distribution. A KS p -value of 0.05 means that we can exclude the possibility that the tested distribution is not a normal distribution with a 95% confidence level. The higher the p -value, the better its match with a normal distribution.

We use two different durations, $d_T = 64$ s and $d_T = 4092$ s, and two different sampling rates, $f_s = 2048$ Hz and $f_s = 16$ kHz. Normally, we split data into trunks of equal duration, for example, 4 s. Then we average the ACFs or the PSDs that are estimated from these trunks. We also need to truncate the ACF to the duration that we need, for example, $d_t = 0.5$ s. This indicates that we assume that the duration of the GW signal is enclosed within d_t .

The stationary Gaussian noise $n(t)$ follows a multivariate normal distribution, $n \sim \mathcal{N}(\mu, \mathcal{C})$, where μ is the mean value and \mathcal{C} is the covariance matrix, which is a Toeplitz matrix based on the ACF. We follow Isi and Farr [6] to Cholesky-decompose the covariance matrix into a lower-triangular matrix L and its transpose L^\top ,

$$\mathcal{C} = LL^\top. \quad (5)$$

The whitened noise can be written as

$$\bar{n}(t) = L^{-1}n(t). \quad (6)$$

In the application of KS test, we partitioned the strain data into multiple segments of equivalent duration, specifically 4 s. Consequently, for each method and setting, a set of segmented data was obtained. This allows us to compute an array of p -values and establish a distribution derived from the KS test. We discard the truncated data that include the chirp signal, which means that we only calculate the p -value for the off-source data. If the ACF describes the noise well, p -values follow a rather flat distribution and most of them should be greater than 0.05.

In Fig. 1, we show the effect of the total duration d_T and the sampling rate on different methods. The durations of the truncated data are $d_t = 0.5$ s and $d_t = 4$ s for TD methods and the FD method, respectively. We can see that all the results of the FD method indicate that the PSDs describe the noise well. However, for the results of the TTD1 method, whose truncated ACF is obtained from Eq. (3), almost all of them fail the KS test. For the results of the TTD2 method, whose truncated ACF is obtained from Eq. (4), only the case with a duration of 64 s and a sampling rate of 16 kHz fails the KS test. Compared with the results of Fig. 2, which will be introduced later, it may seem strange that when the total duration is $d_T = 64$ s and the sampling rate is

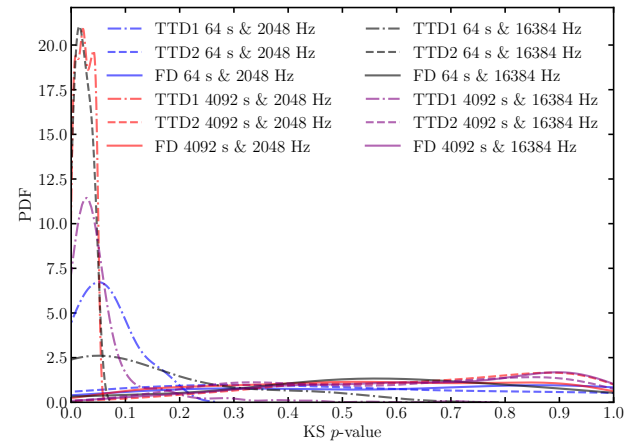


FIG. 1: The distributions of the KS p -value for three methods with different settings. For each method (same line style), we show the results of four different settings in different colors. The labels in the legend represent the method used to obtain the ACF, the total duration of the GW data d_T , and the sampling rate f_s .

16 kHz, the results of the TTD2 method do not seem to describe the noise well. We find that this may be caused by the short total duration, because the results become similar to those of the FD cases when we set the total duration to $d_T = 128$ s. This highlights the importance of the total duration d_T , as it affects the estimation of the ACF.

B. SNR estimations

Another way to check the consistency among different settings is to compare the SNRs of a GW190521-like signal. First, we generate the waveform in TD, which can be written as $h(t, \lambda)$ where t is the time and λ represents the parameters of the waveform. The source parameters for the SNR calculations are listed in Table I. We use the IMRPhenomXPHM waveform model [34] from LALSuite [35, 36]. For TTD methods, it is easy to calculate the SNR based on Eq. (2) and Eq. (5),

$$\rho^2 = (L^{-1}h(t, \lambda))^\top (L^{-1}h(t, \lambda)). \quad (7)$$

For the FD method, we use FFT to transform the TD waveform to FD and then calculate the SNR with

$$\rho^2 = \langle h(f, \lambda) | h(f, \lambda) \rangle. \quad (8)$$

As mentioned above, our GW190521-like event contains the full IMR signal, although the inspiral of which is quite short. So there is no abrupt start or end for this signal and we expect different methods to give the same result. When we calculate SNRs using different methods, the trigger time of the signal always locates in the centre of the data. Furthermore, we take the results of the FD method as the true value, for this method is mature and

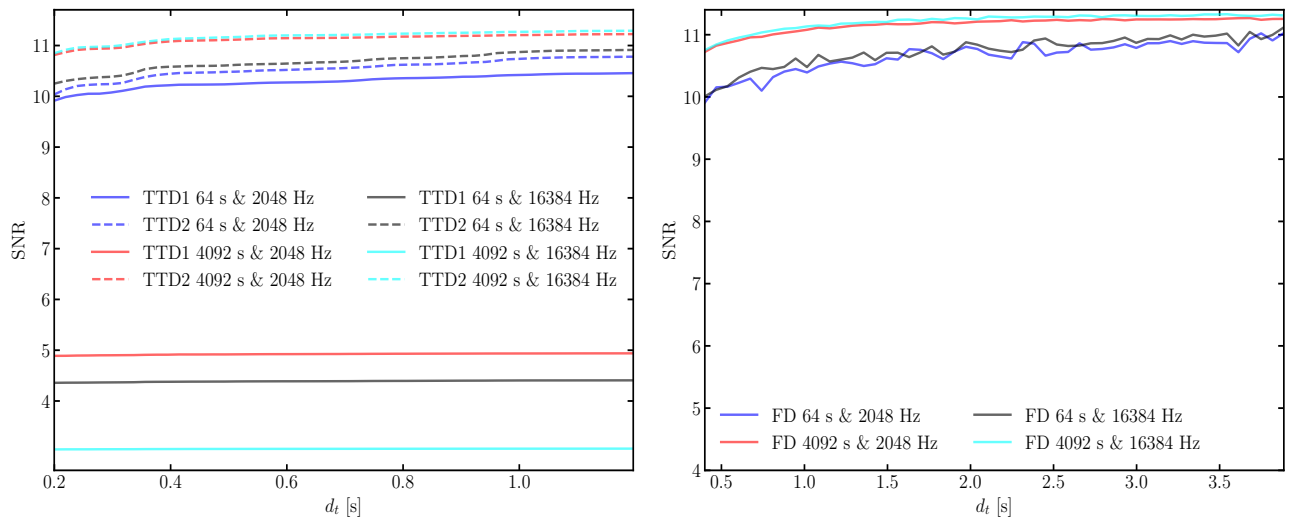


FIG. 2: SNRs of a GW190521-like signal, varying with different durations of the truncated data d_t . We show results based on ACFs from three different methods, with different total durations d_T and different sampling rates f_s .

sufficiently verified. This is also supported by the results in Fig. 1 and Fig. 2.

Moreover we investigate the effect of the duration of the truncated data d_t in Fig. 2, where d_t is also the duration of the signal generated by the waveform model. In Fig. 2, the TTD1 method provides large variance of SNRs. The mean relative error of this method is approximately 73%, indicating potential inadequacies in the handling of ACF estimation within the TTD1 method. In contrast, the Welch method exhibits greater reliability when applied to smaller data sets and demonstrates less susceptibility to nonstationarities.

From Fig. 2, we find that the sampling rate has little effect on the SNRs of a GW190521-like signal. The mean relative errors between the SNRs of the FD method with different sampling rates are all smaller than 0.8%. For the SNRs of the TTD2 method, the mean relative errors between different sampling rates are smaller than 5%. If we only change the total duration d_T for different methods, the mean relative errors of the SNRs are approximately 5% for TTD2 and FD methods. The results of TTD2 and FD methods show that a larger d_T gives a better estimate of the SNR. The SNRs of the 64-s long GW data are underestimated compared to the 4092-s long cases. It should be noted that the duration of the truncated data d_t also affects the results of different methods. For these methods, the relative error of SNRs between the smallest d_t and the largest d_t ranges from 4% to 11%.

IV. BAYESIAN INFERENCE

We now have a basic idea of how to use the TD method. One of the main points is that it should be performed with sufficiently long durations for both d_T and d_t . An-

other important point is that the ACF estimated by the TTD1 method may be biased in some improper setting. To further investigate the consistency between two TD methods and the FD method, we compare results of Bayesian inferences from these different methods. Specifically, we use a total duration of GW data $d_T = 4092$ s and a sampling rate $f_s = 2048$ Hz for TD and FD methods. We select this particular configuration of duration and sampling rate due to its superior performance in both the KS test and SNR comparison, as detailed in Sec. III. Furthermore, this choice aligns with the settings used in Ref. [37], demonstrating consistent results across different sampling rates.

The durations of the truncated data are $d_t = 0.8$ s and $d_t = 4$ s for the TD and FD methods respectively. Note that d_t also represents the duration of the signal generated by the waveform model. On the one hand, the average relative error of the SNRs between the FD method and the TTD2 method is approximately 0.3%, which is negligible. Thus, we expect similar results from Bayesian inference using these two methods. On the other hand, if one performs Bayesian inference with the biased ACF given by the TTD1 method, we anticipate significantly different results.

In this section, we first introduce the Bayes theorem and some basic settings for Bayesian inference. Then we show results based on more reasonable PSDs, where the PSD is estimated by the PyCBC package.

A. Settings

To estimate the parameters λ of GW190521 under a specific waveform model $h(\lambda)$, we use the Bayesian infer-

ence based on the Bayes theorem,

$$P(h(\lambda)|d, I) = \frac{P(d|h(\lambda), I)P(h(\lambda)|I)}{P(d|I)}, \quad (9)$$

where $P(h(\lambda)|d, I)$ is the posteriors of the parameters, $P(h(\lambda)|I)$ is their priors, $P(d|h(\lambda), I)$ is the likelihood, and $P(d|I)$ is the evidence. Note that the evidence of a specific model is a constant. According to Finn [38], the likelihood can be written as,

$$\begin{aligned} P(d|h(\lambda), I) &= P(d - h(\lambda)|I) \\ &= \exp \left[-\frac{1}{2} \langle d - h(\lambda) | d - h(\lambda) \rangle \right]. \end{aligned} \quad (10)$$

It is worth noting that, for the TD and FD methods, we calculate the likelihood according to Eq. (2) and Eq. (1), respectively. For multiple detectors, one can simply multiply their likelihoods together.

We impose uniform priors on the redshifted component masses, and we sample from the redshifted chirp mass and the mass ratio in ranges of $(10, 200) M_{\odot}$ and $(0.04, 1)$, respectively. The prior on the luminosity distance is uniform in the co-moving volume, with a range of $(50, 10^4)$ Mpc. For other parameters, we use the same priors as those used by the LVK Collaboration [3].

We then implement the likelihood using the `Bilby` (version 1.2.1) package [39] and perform Bayesian inference using the `dynesty` sampler [40] with 1000 live points. The minimum (walks) and maximum numbers of sampling steps (maxmcmc) are 100 and 5000, respectively.

B. Results

We perform the Bayesian inference using the FD method, the TTD1 method, and the TTD2 method. Note that the downsampling algorithm and the high-pass algorithm used here are implemented in the `PyCBC` package. We compare posteriors from these three methods in Fig. 3. As expected, the FD method and the TTD2 method give similar posterior distributions for almost all parameters. Furthermore, the log-Bayes factor between them is less than 0.1, indicating that we can ignore the differences. We have also tried a duration of 1 s for the truncated ACF of the TTD2 method and obtained similar results.

However, for the TTD1 method, the results are quite different from those of the FD method and the TTD2 method. The estimation of most parameters, such as the chirp-mass and the luminosity distance, seems highly biased. Furthermore, the log-Bayes factor between the TTD1 method and the FD method is $\log_{10} \mathcal{B}_{\text{FD}}^{\text{TTD1}} \approx -18$. This means that the results from the TTD1 method are very different from the FD and TTD2 methods. This also agrees with what we expected that, a biased ACF due to the improper setting of the TTD1 method leads to biased estimations.

The parameter-estimation results are summarised in Table I. To quantify the differences between the results of those two TTD methods and the FD method, we calculate the Kullback-Leibler divergence (KLD) and the Jensen-Shannon divergence (JSD) between the posterior samples of them. For two posterior distributions p and q , the KLD of them is defined by

$$D_{\text{KL}}(p(x)|q(x)) = \int p(x) \log_2 \left[\frac{p(x)}{q(x)} \right] dx, \quad (11)$$

and the JSD of them is defined by

$$D_{\text{JS}}(p, q) = \frac{1}{2} \left(D_{\text{KL}}(p|s) + D_{\text{KL}}(q|s) \right), \quad (12)$$

where $s = (p + q)/2$. As we can see in Table I, for the TTD2 method, all JSD values are less than 0.07, which means that it is acceptable to assume that the difference between the results of these two methods is negligible. However, for the TTD1 method, almost all JSD values are greater than 0.07. Thus, we conclude that, given current settings, the TTD1 method gives very different results, compared to the other two methods.

V. DISCUSSION AND CONCLUSION

In this paper, we investigate the performance of the TD Bayesian inference. We take the FD Bayesian inference as a comparison when analysing the GW190521 signal, which lasts for only 0.1 s. This event can be analysed by both the TD and FD methods. Note that such a comparison cannot be made with a ringdown signal alone due to its abrupt start, nor can it currently be performed on a much longer signal due to the computational cost of calculating the inverse of the covariance matrix. For example, for a 1-s long signal, the dimension of the covariance matrix will be as large as 16384×16384 when the sampling rate is 16384 Hz. The speed of calculating the likelihood is limited by the computational cost, even if we compute the inverse of the covariance matrix using the Cholesky method.

One of the key points of this investigation is how a truncated ACF can describe the noise as well as a circular ACF does. Therefore, we calculate the KS p -values with two truncated ACFs and one circular ACF, which are for the TTD method and the FD method, respectively. We use them to calculate SNRs for a GW190521-like signal generated with the IMRPhenomXPHM waveform model. Compared to the results of the FD method, the results of the TTD2 method are more reliable than those of the TTD1 method. Specifically, the largest relative error between the SNRs of the TTD1 and FD methods is approximately 73% with a non-optimal setting. Furthermore, almost all ACFs for the TTD1 method fail in the KS test. Note that one of the ACFs for the TTD2 method also fails in the KS test when the total duration d_T is not long enough.

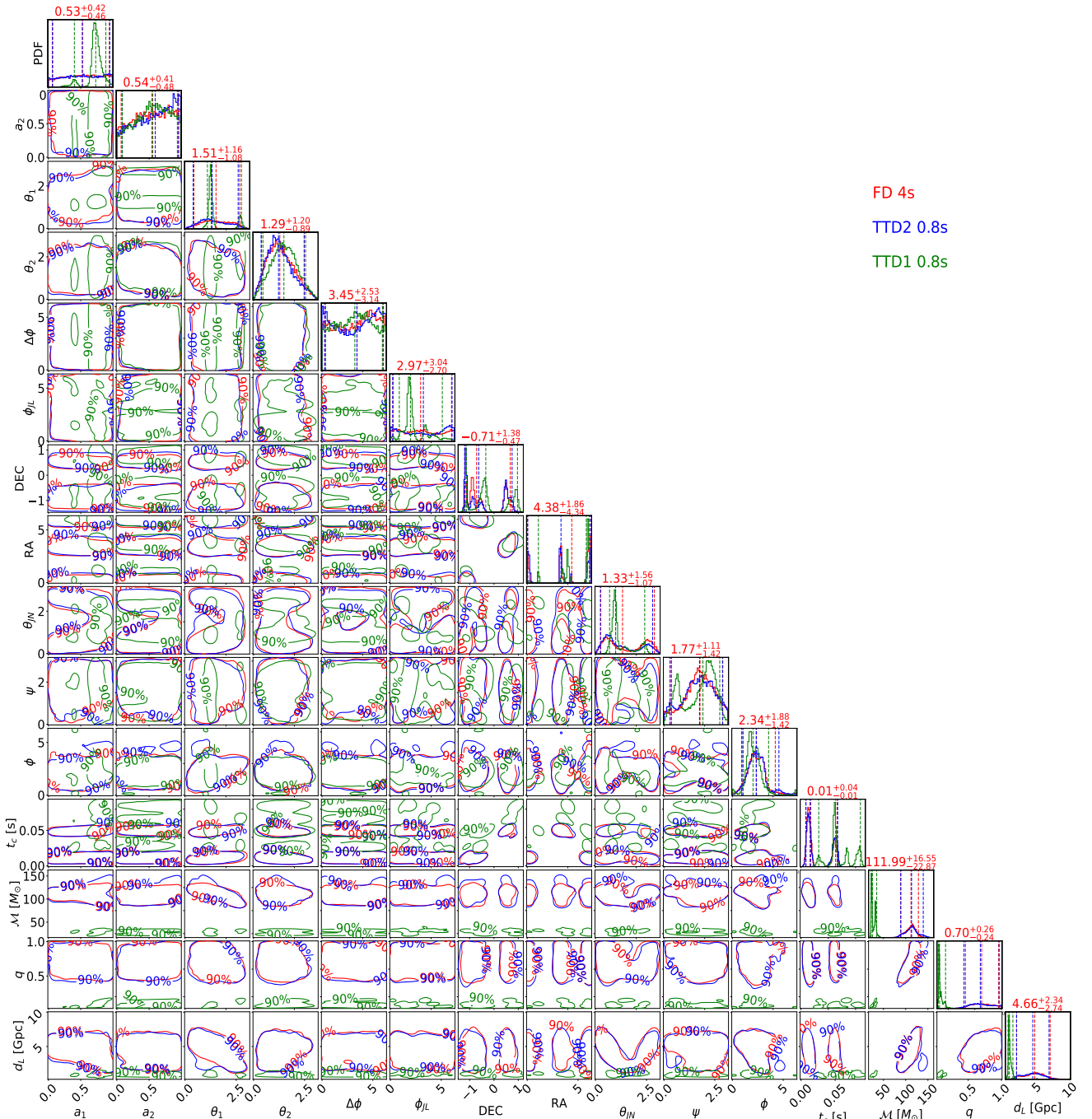


FIG. 3: Posterior distributions for the parameters of GW190521 from three methods: the FD method (red), the TTD1 method (green), and the TTD2 method (blue). The durations for the FD method and two TD methods are 4 s and 0.8 s, respectively. The contours represent the 90% credible level. The numbers on the diagonal are the median values and the 90% credible measurements of each parameter in the FD method.

The key factors in our comparison are the total duration d_T for the noise estimation, the duration of the truncated data d_t , and the sampling rate f_s . For the total duration d_T , we find that $d_T = 64$ s is not long enough for the analysis of a GW190521-like signal. The relative error caused by this factor can be up to 5% for the TTD2 method. For the sampling rate, its effect is neg-

ligible if the adopted total duration d_T is large enough, i.e. $d_T = 4092$ s in our case. For the duration of the truncated data d_t , the relative error can be as large as 11%. From these analyses, it is concluded that the TTD2 method should be performed with sufficiently long durations for both d_T and d_t , i.e., $d_t = 0.8$ s and $d_T = 4092$ s for a GW190521-like signal.

TABLE I: The second column, the third column, and the sixth column show, respectively for the FD method, the TTD2 method, and the TTD1 method, the medians and errors at the 90% credible level for the parameters of GW190521. To quantify the differences between results of these three methods, we calculate the KLD and JSD between their posterior samples against the FD method. The parameters in the ninth column are used to calculate SNRs as described in Sec. III B. The definition of these parameters is the same as that used in the `Bilby` package.

	FD	TTD2	KLD	JSD	TTD1	KLD	JSD	Injection
a_1	$0.53^{+0.42}_{-0.46}$	$0.53^{+0.42}_{-0.47}$	0.013	0.003	$0.73^{+0.16}_{-0.33}$	1.387	0.341	0.70
a_2	$0.54^{+0.41}_{-0.48}$	$0.59^{+0.36}_{-0.51}$	0.028	0.007	$0.56^{+0.38}_{-0.47}$	0.024	0.006	0.96
θ_1	$1.51^{+1.16}_{-1.08}$	$1.32^{+1.28}_{-0.92}$	0.041	0.010	$1.27^{+1.48}_{-0.18}$	2.327	0.440	1.07
θ_2	$1.29^{+1.2}_{-0.89}$	$1.22^{+1.25}_{-0.85}$	0.021	0.005	$1.49^{+1.06}_{-1.02}$	0.067	0.016	1.54
$\Delta\phi$	$3.45^{+2.53}_{-3.14}$	$3.43^{+2.59}_{-3.18}$	0.020	0.005	$3.23^{+2.71}_{-2.87}$	0.029	0.007	0.52
ϕ_{JL}	$2.97^{+3.04}_{-2.7}$	$3.24^{+2.82}_{-3.02}$	0.051	0.013	$1.97^{+3.14}_{-1.1}$	0.950	0.215	3.47
DEC	$-0.71^{+1.38}_{-0.47}$	$-0.63^{+1.37}_{-0.58}$	0.288	0.068	$-0.34^{+1.3}_{-0.8}$	1.731	0.383	0.68
RA	$4.38^{+1.86}_{-4.34}$	$3.32^{+2.92}_{-3.27}$	0.164	0.043	$5.81^{+0.3}_{-4.71}$	1.817	0.364	3.51
θ_{JN}	$1.33^{+1.56}_{-1.07}$	$0.99^{+1.81}_{-0.74}$	0.084	0.021	$0.99^{+1.42}_{-0.3}$	1.733	0.321	1.66
ψ	$1.77^{+1.11}_{-1.42}$	$1.75^{+1.14}_{-1.45}$	0.022	0.006	$1.91^{+0.83}_{-1.54}$	0.230	0.056	2.32
ϕ	$2.34^{+1.88}_{-1.42}$	$2.37^{+2.21}_{-1.42}$	0.029	0.007	$2.03^{+1.53}_{-0.95}$	0.227	0.052	2.09
t_c [s]	$t_0^{+0.040}_{-0.006}$	$t_0^{+0.041}_{-0.006}$	0.040	0.010	$t_0 + 0.038^{+0.036}_{-0.025}$	0.987	0.612	t_0
\mathcal{M} [M_\odot]	$111.99^{+16.55}_{-22.87}$	$113.24^{+26.21}_{-24.42}$	0.097	0.029	$25.23^{+9.63}_{-3.05}$	0.0	1.0	126.6
q	$0.70^{+0.26}_{-0.24}$	$0.68^{+0.28}_{-0.24}$	0.027	0.007	$0.07^{+0.09}_{-0.02}$	0.015	0.996	0.89
d_L [Gpc]	$4.7^{+2.3}_{-2.7}$	$4.4^{+2.5}_{-2.4}$	0.033	0.008	$0.8^{+0.5}_{-0.2}$	0.755	0.928	2.75

*Note: $t_0 = 1242442967.413$ s is the trigger time of GW190521.

To further verify our results, we perform Bayesian inference using two TD methods and the FD method. For two TD methods (TTD1 method and TTD2 method), we set $d_t = 0.8$ s and $d_T = 4092$ s. For the FD method, we set $d_t = 4$ s and $d_T = 4092$ s. We confirm that, for the TTD2 method and the FD method, they have similar results, and the log-Bayes factor between their posteriors is less than 0.1. The JSD values of each parameter between these two methods are all less than 0.07, meaning that the difference between them is negligible.

For the TTD1 method and the FD method, the log-Bayes factor between them is about -18 , and the JSD values of most parameters are larger than 0.07. However, we cannot conclude that the TTD1 method itself is not reliable. It is posited that consistent outcomes can be achieved given the correct handling of the data. This assertion is substantiated by Fig. 1 and Fig. 2, which illustrate results obtained from a total duration of 4092 s at a sampling rate of 2048 Hz, demonstrating consistency between the TTD1 method and the FD method. The reliability of the TTD1 method under different settings can further be verified through a KS test, as detailed in Sec. III A. We do not delve deeply into this since the TTD2 method is both reliable and accessible. We here

aim to present results of the biased TTD1 method for comparison. Overall, this analysis highlights the importance of performing the consistency check between different methods.

The TTD method is widely used in ringdown analysis. Here, we show that it can also be used in the full IMR analysis only when we handle it with extra care. Furthermore, our analyses are helpful to understand the inconsistency between the results of Ref. [14] and Ref. [15]. Based on our analyses, we got consistent results for ringdown analyses of GW150914 with different sampling frequencies, as shown in Ref. [37]. To allow for reproducibility, we have released codes for noise estimation at Ref. [41].

ACKNOWLEDGMENTS

We thank Yi-Ming Hu for insightful discussions and the anonymous referee for constructive comments. This work was supported by the China Postdoctoral Science Foundation (2022TQ0011), the National Natural Science Foundation of China (12247152, 11975027, 11991053, 11721303), the National SKA Program of China (2020SKA0120300), the Beijing Municipal Natu-

ral Science Foundation (1242018), the Max Planck Partner Group Program funded by the Max Planck Society, and the High-performance Computing Platform of Peking University. HTW is supported by the Opening Foundation of TianQin Research Center.

This research has made use of data or software obtained from the Gravitational Wave Open Science Center (gwosc.org), a service of LIGO Laboratory, the LIGO Scientific Collaboration, the Virgo Collaboration, and KAGRA [42]. LIGO Laboratory and Advanced LIGO are funded by the United States National Science Foundation (NSF) as well as the Science and Technology Facilities Council (STFC) of the United Kingdom, the Max-Planck-Society (MPS), and the State of Niedersachsen/Germany for support of the construction of Ad-

vanced LIGO and construction and operation of the GEO600 detector. Additional support for Advanced LIGO was provided by the Australian Research Council. Virgo is funded, through the European Gravitational Observatory (EGO), by the French Centre National de Recherche Scientifique (CNRS), the Italian Istituto Nazionale di Fisica Nucleare (INFN) and the Dutch Nikhef, with contributions by institutions from Belgium, Germany, Greece, Hungary, Ireland, Japan, Monaco, Poland, Portugal, Spain. KAGRA is supported by Ministry of Education, Culture, Sports, Science and Technology (MEXT), Japan Society for the Promotion of Science (JSPS) in Japan; National Research Foundation (NRF) and Ministry of Science and ICT (MSIT) in Korea; Academia Sinica (AS) and National Science and Technology Council (NSTC) in Taiwan of China.

[1] M. Isi and W. M. Farr, arXiv e-prints , arXiv:2202.02941 (2022), arXiv:2202.02941 [gr-qc].

[2] B. P. Abbott *et al.* (LIGO Scientific Collaboration and Virgo Collaboration), *Phys. Rev. X* **9**, 031040 (2019).

[3] R. Abbott *et al.*, *Phys. Rev. X* **11**, 021053 (2021), arXiv:2010.14527 [gr-qc].

[4] R. Abbott *et al.* (KAGRA, VIRGO, LIGO Scientific), *Phys. Rev. X* **13**, 041039 (2023), arXiv:2111.03606 [gr-qc].

[5] B. P. Abbott *et al.* (LIGO Scientific, Virgo), *Class. Quant. Grav.* **37**, 055002 (2020), arXiv:1908.11170 [gr-qc].

[6] M. Isi and W. M. Farr, arXiv e-prints , arXiv:2107.05609 (2021), arXiv:2107.05609 [gr-qc].

[7] C. V. Vishveshwara, *Phys. Rev. D* **1**, 2870 (1970).

[8] W. H. Press, *Astrophys. J. Lett.* **170**, L105 (1971).

[9] S. A. Teukolsky, *Astrophys. J.* **185**, 635 (1973).

[10] E. Finch and C. J. Moore, *Phys. Rev. D* **104**, 123034 (2021), arXiv:2108.09344 [gr-qc].

[11] E. Finch and C. J. Moore, *Phys. Rev. D* **106**, 043005 (2022), arXiv:2205.07809 [gr-qc].

[12] J. C. Bustillo, P. D. Lasky, and E. Thrane, *Phys. Rev. D* **103**, 024041 (2021).

[13] C. D. Capano, J. Abedi, S. Kastha, A. H. Nitz, J. Westerweck, Y.-F. Wang, M. Cabero, A. B. Nielsen, and B. Krishnan, (2022), arXiv:2209.00640 [gr-qc].

[14] M. Isi, W. M. Farr, M. Giesler, M. A. Scheel, and S. A. Teukolsky, *Phys. Rev. Lett.* **127**, 011103 (2021), arXiv:2012.04486 [gr-qc].

[15] R. Cotesta, G. Carullo, E. Berti, and V. Cardoso, *Phys. Rev. Lett.* **129**, 111102 (2022), arXiv:2201.00822 [gr-qc].

[16] B. P. Abbott *et al.* (LIGO Scientific Collaboration and Virgo Collaboration), *Phys. Rev. Lett.* **116**, 061102 (2016).

[17] R. Abbott *et al.* (LIGO Scientific Collaboration and Virgo Collaboration), *Phys. Rev. Lett.* **125**, 101102 (2020), arXiv:2009.01075 [gr-qc].

[18] M. Isi, M. Giesler, W. M. Farr, M. A. Scheel, and S. A. Teukolsky, *Phys. Rev. Lett.* **123**, 111102 (2019), arXiv:1905.00869 [gr-qc].

[19] R. Abbott *et al.* (LIGO Scientific, Virgo), *Phys. Rev. D* **103**, 122002 (2021), arXiv:2010.14529 [gr-qc].

[20] R. Abbott *et al.* (LIGO Scientific, VIRGO, KAGRA), arXiv e-prints , arXiv:2112.06861 (2021), arXiv:2112.06861 [gr-qc].

[21] H.-T. Wang, S.-P. Tang, P.-C. Li, and Y.-Z. Fan, *Phys. Rev. D* **104**, 104063 (2021), arXiv:2104.07594 [gr-qc].

[22] M. H.-Y. Cheung, L. W.-H. Poon, A. K.-W. Chung, and T. G. F. Li, *JCAP* **02**, 040 (2021), arXiv:2002.01695 [gr-qc].

[23] A. K. Mishra, A. Ghosh, and S. Chakraborty, *Eur. Phys. J. C* **82**, 820 (2022), arXiv:2106.05558 [gr-qc].

[24] P. Hu, K. Jani, K. Holley-Bockelmann, and G. Carullo, (2021), arXiv:2112.06856 [gr-qc].

[25] M. Punturo, M. Abernathy, *et al.*, *Class. Quantum Grav.* **27**, 194002 (2010).

[26] D. Reitze, R. X. Adhikari, *et al.*, in *Bull. Am. Astron. Soc.*, Vol. 51 (2019) p. 35, arXiv:1907.04833 [astro-ph.IM].

[27] P. Amaro-Seoane, H. Audley, S. Babak, J. Baker, *et al.*, ArXiv e-prints , arXiv:1702.00786 (2017), arXiv:1702.00786 [astro-ph.IM].

[28] J. Luo *et al.* (TianQin), *Class. Quant. Grav.* **33**, 035010 (2016), arXiv:1512.02076 [astro-ph.IM].

[29] J. Mei *et al.* (TianQin), *PTEP* **2021**, 05A107 (2021), arXiv:2008.10332 [gr-qc].

[30] W.-R. Hu and Y.-L. Wu, *National Science Review* **4**, 685 (2017).

[31] B. Allen, W. G. Anderson, P. R. Brady, D. A. Brown, and J. D. E. Creighton, *Phys. Rev. D* **85**, 122006 (2012), arXiv:gr-qc/0509116 [gr-qc].

[32] M. Khan and S. Agha, *Analog Integrated Circuits and Signal Processing* **105**, 99 (2020).

[33] P. D. Welch, *IEEE Trans. Audio & Electroacoust* **15** (1967), 10.1109/TAU.1967.1161901.

[34] G. Pratten, C. García-Quirós, M. Colleoni, A. Ramos-Buades, H. Estellés, M. Mateu-Lucena, R. Jaume, M. Haney, D. Keitel, J. E. Thompson, and S. Husa, *Phys. Rev. D* **103**, 104056 (2021), arXiv:2004.06503 [gr-qc].

[35] LIGO Scientific Collaboration, “*LIGO Algorithm Library - LALSuite*,” free software (GPL) (2018).

- [36] K. Wette, *SoftwareX* **12**, 100634 (2020).
- [37] H.-T. Wang and L. Shao, *Phys. Rev. D* **108**, 123018 (2023), arXiv:2311.13300 [gr-qc].
- [38] L. S. Finn, *Phys. Rev. D* **46**, 5236 (1992), arXiv:gr-qc/9209010 [gr-qc].
- [39] G. Ashton *et al.*, *ApJS* **241**, 27 (2019).
- [40] J. S. Speagle, *MNRAS* **493**, 3132 (2020), arXiv:1904.02180 [astro-ph.IM].
- [41] H. Wang and L. Shao, , https://github.com/whaitian/FD_TD_IMR.git (2023).
- [42] R. Abbott *et al.* (KAGRA, VIRGO, LIGO Scientific), *Astrophys. J. Suppl.* **267**, 29 (2023), arXiv:2302.03676 [gr-qc].